minerals

MDPI

Article

Investigation of Cerium Reduction Efficiency by Grinding with Microwave Irradiation in Mechanochemical Processing

Tatsuya Kato [1,2], Motonori Iwamoto [3] and Chiharu Tokoro [1,4,*]

[1] Faculty of Science and Engineering, Waseda University, 3-4-1 Okubo, Shinjuku-ku, Tokyo 169-8555, Japan; kato.tatsuya@nitech.ac.jp
[2] Department of Physical Science and Engineering, Nagoya Institute of Technology, Gokisocho, Showa Ward, Nagoya 466-8555, Japan
[3] Powder Technology Center, Nippon Coke & Engineering Co., Ltd., 1 Koh-machi, Tochigi 328-8503, Japan; motonori-iwamoto@n-coke.com
[4] Faculty of Engineering, The University of Tokyo, 7-3-1 Hongo, Bunkyo-ku, Tokyo 113-8656, Japan
* Correspondence: tokoro@waseda.jp; Tel.: +81-3-5286-3320

Abstract: This study evaluated the efficiency of cerium reduction by grinding with microwave irradiation in mechanochemical processing. Grinding experiments with microwave irradiation were conducted using an agitating mixer. Since the structure of the ground samples was amorphous and the cerium concentration was much lower than those of other elements, the valence change and structural change of cerium after grinding with microwave irradiation were investigated using X-ray absorption fine structure (XAFS) analysis in the cerium K-edge. The X-ray absorption near-edge structure (XANES) analysis revealed that a portion of tetravalent cerium was reduced to trivalent cerium by grinding with microwave irradiation. In addition, it was confirmed by extended X-ray absorption fine structure (EXAFS) analysis that oxygen vacancies were produced as a result of the cerium reduction reaction. To evaluate the efficiency of cerium reduction efficiency, the percentage reduction by grinding with microwave irradiation was compared to that by planetary ball milling and microwave irradiation. As a result, it was revealed that the efficiency of cerium reduction via grinding with microwave irradiation was higher than that via microwave irradiation and the same as that via planetary ball milling. Moreover, a larger amount of tetravalent cerium could be reduced to trivalent cerium by grinding with microwave irradiation than when using planetary ball milling and microwave irradiation.

Keywords: X-ray absorption fine structure; extended X-ray absorption fine structure; local structure; oxygen vacancy; mechanochemistry

Citation: Kato, T.; Iwamoto, M.; Tokoro, C. Investigation of Cerium Reduction Efficiency by Grinding with Microwave Irradiation in Mechanochemical Processing. *Minerals* **2022**, *12*, 189. https://doi.org/10.3390/min12020189

Academic Editor: Konstantinos Komnitsas

Received: 7 December 2021
Accepted: 28 January 2022
Published: 31 January 2022

1. Introduction

During the past two decades, the mechanochemical reactions caused by high-intensity grinding have attracted increasing academic and commercial attention. This is due to the fact that mechanochemical reactions offer rapid, cleaner alternatives to the conventional chemical reactions used in nanomaterials, waste recycling, and mineral processing [1–12]. The use of mechanochemical reactions is also known as mechanochemical processing or mechanical activation [2]. The phenomenon of a mechanochemical reaction corresponding to high-intensity grinding for many materials is widely recognized [1–6]. In addition, the process of mechanochemical reaction has recently been investigated and revealed by X-ray diffraction analysis (XRD), kinetics, and X-ray absorption fine structure (XAFS) analysis [13–18]. However, despite the wide recognition of mechanochemical processing by high-intensity grinding and its benefits, the development and optimization of attractive proof-of-principle laboratory experiments into viable large-scale processes have not come to pass [1,12].

In many of the previous studies [7–11], a planetary ball mill is commonly used to cause the mechanochemical reaction for many kinds of grinding samples. However, a planetary ball mill is commonly used not on a large scale but a laboratory scale, due to the high energy densities and low acquisition costs [19]. Several researchers reported a scaling-up method for planetary ball mills, based on a discrete element method (DEM) simulation [20,21]. However, the development of large-scale planetary ball mills was problematic, and they cannot as yet be implemented. Thus, the development of alternative mills as a substitute for planetary ball mills is desirable.

In this study, mechanochemical processing by grinding with microwave irradiation using an agitating mixer has attracted attention as a substitute for planetary ball milling. Microwave irradiation is known to be one of the factors that cause mechanochemical reactions [22,23]. Comparing microwave irradiation and mechanochemical processing via ball milling, Ribeiro et al. [23] reported that mechanochemical processing by ball milling was a more effective procedure than microwave irradiation in terms of catalyst preparation and the catalytic reaction. However, it was reported that the most effective processes for the catalytic oxidation of cyclohexane were a combination of microwave irradiation and mechanochemical processing by ball milling [23]. According to this study, it is possible for grinding with microwave irradiation to become a more effective process than planetary ball milling.

Weathered residual rare-earth ore is considered to be an alternative source of rare-earth minerals [13]. In our previous paper, we reported that cerium dissolution was increased by a mechanochemical reaction corresponding to planetary ball milling [13]. In addition, the cerium reduction reaction (Equation (1)) occurred as a mechanochemical reaction during planetary ball milling [13,14]. The structural change and mechanism of the cerium reduction reaction were revealed using XAFS analysis in our previous paper [14]. Since the mechanochemical phenomenon and its mechanism have already been revealed for weathered residual rare-earth ore, this ore was selected as a target material in this study. The cerium reduction reaction is as follows:

$$CeO_2 \rightarrow CeO_{2-x} + \frac{x}{2}O_2 \quad (1)$$

The objective of this study is to evaluate cerium reduction efficiency via mechanochemical processing, by grinding with microwave irradiation using an agitating mixer. First, the weathered residual rare-earth ore was ground by an agitating mixer with microwave irradiation. Next, the valence change and structural change of ground samples after grinding with microwave irradiation were investigated, using XAFS analysis in cerium K-edge since the structure of the ground samples was amorphous and the cerium concentration was much lower than that of other elements. Finally, the cerium reduction efficiency by grinding with microwave irradiation was compared with that by planetary ball milling and microwave irradiation to evaluate the cerium reduction efficiency.

2. Materials and Methods

2.1. Analysis

The detailed analysis methods for weathered residual rare-earth ore were described in our previous paper [13]. Briefly, the major chemical composition of this ore was determined by X-ray fluorescence (XRF; ZSX PrimusIII+, Rigaku Corporation, Tokyo, Japan) while the concentrations of rare-earth elements were analyzed by laser ablation inductively coupled plasma mass spectrometry (LA-ICP-MS; 7500 Series, Agilent Technologies, Santa Clara, CA, USA). The mineral composition in this ore was revealed by mineral liberation analysis (MLA; QuantaF Co., FEI, Hillsboro, OR, USA).

2.2. Heating Experiments by Microwave Irradiation

Heating experiments by microwave irradiation were performed using a microwave irradiation device (μReactor EX, Shikoku Instrumentation Co. Ltd., Kagawa, Japan) under

atmospheric conditions. Each experiment heated 10 g ore. The increasing speed was fixed at 2 °C/min and the ore was kept for 1 h at the target temperatures. After experiments, the samples cooled naturally. The target temperature was set at 700, 900, 950, and 1100 °C. During heating experiments, the output of the microwave was monitored every second. Based on this information, the energy consumption was calculated.

2.3. Grinding Experiments by Planetary Ball Mill

Grinding experiments using a planetary ball mill (PM100, Verder Scientific Co. Ltd., Tokyo, Japan) were performed under the same conditions, as reported in our previous paper [13]. The experimental results are quoted from our previous papers [13]. Each grinding experiment ground 100 g of ore. The rotation speed of the mill was fixed at 300 rpm and 25 chrome steel balls, with a diameter of 19 mm, were used as the grinding medium. The grinding times were set at 10, 60, and 720 min. The volume of the mill was 0.5 dm^3. During grinding experiments with the planetary ball mill, the energy consumption of the planetary ball mill was monitored.

2.4. Grinding Experiments with Microwave Irradiation

Grinding experiments with microwave irradiation were conducted using an agitating mixer (FM20, Nippon Coke & Engineering Co. Ltd., Tokyo, Japan). Each experiment ground 1000 g of ore. The rotation speed of the mill was fixed at 200 rpm. Grinding time was set at 60, 180, and 420 min. The reaction temperature was fixed at 250 °C. The volume of the mixer was 20 dm^3. During grinding experiments with microwave irradiation, the energy consumption was monitored using the same method as for the planetary ball mill.

2.5. X-ray Absorption Fine Structure Analysis of the Cerium L_{III}- and K-Edge

The conditions of XAFS analysis of the cerium LIII edge were as already described in our previous papers [13,14]. Briefly, XAFS analysis of the cerium LIII edge was performed using the BL5S1 beamline in the Aichi Synchrotron Radiation Center, Japan. The X-ray absorption near-edge structure (XANES) analysis was performed using a range of 5720–5740 eV to reveal the valence of the cerium.

The XAFS analysis at the cerium K-edge was performed using the BL01B1 beamline at the SPring-8 Synchrotron Radiation Facility, Japan. All XAFS spectra at the cerium K-edge were obtained at room temperature. The electron storage ring was operated at 8.0 GeV, with a stored current of 99.5 mA. The energy was from 40130 eV to 41920 eV. The continuous X-ray synchrotron radiation was monochromatized using a silica (311) double-crystal monochromator. The XAFS spectra for all samples were obtained via the fluorescence mode using a 19-element germanium (Ge) solid-state detector. Cerium phosphate ($CePO_4$) and cerium oxide (CeO_2) were used as reference materials.

The EXAFS analysis was conducted under the same conditions as described in our previous paper [14]. Briefly, the EXAFS function was Fourier-transformed from a k^3-weighted EXAFS function to a radial distribution function (RDF) using a Hanning window function of within 1–12 $\times$ 10^{10} m^{-1}. Structural parameters for different coordination shells surrounding both the tri- and tetravalent cerium atom, namely, coordination number, atomic distance, and Debye-Waller factor, were obtained by a curve fitting using both the k^3-weighted EXAFS function and RDF. The structural parameters were obtained after fitting the RDF at an interval of 1.5–4.0 $\times$ 10^{-10} m, consisting of contributions from the first to the fourth coordination shells. The theoretical phase and amplitude function for each shell, as used in curve fitting, were calculated by FEFF 6.0 [24,25]. All EXAFS analysis was performed using Athena and Artemis software [26].

3. Results and Discussion

3.1. Characterization of Weathered Residual Rare-Earth Ore

The detailed characteristics of weathered residual rare-earth ore have already been described in our previous paper [13]. The major chemical composition and concentrations

of rare-earth elements in this ore are shown in Tables 1 and 2. MLA analysis revealed that this ore contained four kinds of cerium minerals; britholite-(Ce) ((Ce, Ca, Th, La, Nd)$_5$(SiO_4, PO_4)$_3$(OH, F)), cerianite ((Ce, Th)O_2), cerite ($Ce_9Fe(SiO_4)_6$[(SiO_3), (OH)](OH)$_3$) and monazite-(Nd) ((Nd, Ce, La)(P, Si)O_4). Among these cerium minerals, britholite-(Ce), cerite and monazite-(Nd) are trivalent cerium minerals, while only cerianite is a tetravalent cerium mineral.

Table 1. Chemical composition of weathered residual rare-earth ore, as analyzed by X-ray fluorescence (mass %) [13].

SiO_2	Fe_2O_3	Al_2O_3	Na_2O	MgO	P_2O_5	K_2O	CaO	TiO_2	MnO	Others
68.6	16.2	7.3	0.3	0.4	0.3	2.1	0.2	0.3	0.2	4.1

Table 2. Concentrations of rare-earth elements in weathered residual rare-earth ore, as analyzed by laser ablation inductively coupled plasma mass spectrometry (mg/dm^3) [13].

Sc	Y	La	Ce	Pr	Nd	Sm	Eu
5.3	1384.1	926.5	2495.5	236.8	903.3	200.0	11.2
Gd	Tb	Dy	Ho	Er	Tm	Yb	Lu
224.2	37.4	236.2	50.4	153.7	23.1	137.9	19.6

3.2. Cerium Reduction by Heating Experiments

The Ellingham diagram of cerium reduction in the range from 0 to 1200 °C is shown in Figure 1 [27]. The standard free energy (ΔG^0, 25 °C, 1 bar) is 330.6 kJ/mol [27]. Since the free energy charge (ΔG) in this area is always a positive value, the cerium reduction reaction did not occur in the range from 0 to 1200 °C.

The XAFS spectra for heating samples corresponding to the XANES region at the cerium L_{III}-edge are shown in Figure 2. In addition, the valence of cerium in each heating sample is shown in Table 3. Above 700 °C, the concentration of trivalent cerium was significantly increased (Table 3). Thus, it was confirmed that the cerium reduction reaction occurred during heating by microwave irradiation from XANES analysis. However, the cerium reduction reaction does not occur as shown in the Ellingham diagram in the range of 0 °C to 1200 °C (Figure 1). In a previous study [28], it was reported that the free energy charge decreased when the lattice defects were present in the structure of cerianite. The weathered residual rare earth ore is very fine-grained because of strong weathering over a long period. Thus, it was suggested that lattice defects occurred naturally in the structure of cerianite in this ore, and cerium reduction reaction occurred more easily.

The structural change of cerianite, corresponding to cerium reduction by heating, was reported in a previous paper [29–32]. The crystal structure of cerianite and cerium trioxide(III) (Ce_2O_3), which is produced after the cerium reduction reaction, corresponds to a fluorite structure (Fm3 m) and a C-type structure (la3), respectively [29–32]. When the cerianite is reduced to Ce_2O_3, eight unit cells of cerianite are synthesized and produce 25% of oxygen vacancy in the structure. This structural change from cerianite to the C-type of Ce_2O_3 involves a mineral reorganization of the skeleton arrangement of the cerium atoms.

Table 3. Concentration of tri- and tetravalent cerium in the heating samples, based on the X-ray absorption near-edge structure analysis of the cerium L_{III} edge (%).

Temperature (°C)	Concentration of Trivalent Cerium	Concentration of Tetravalent Cerium
25	50.7	49.3
700	50.8	49.2
900	51.4	48.6
950	61.0	39.0
1100	75.9	24.1

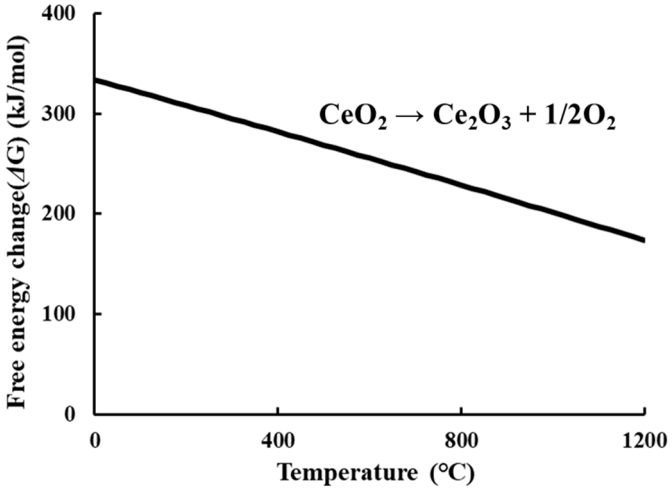

Figure 1. Ellingham diagram of cerium reduction reaction [27].

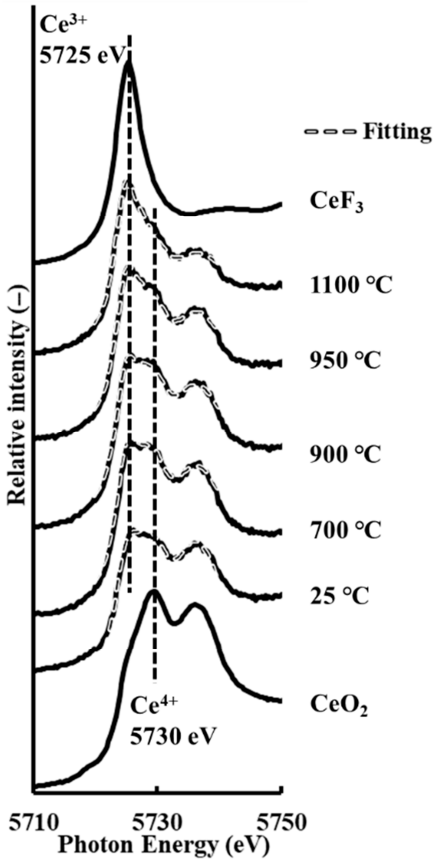

Figure 2. Cerium L_{III} edge X-ray absorption fine structure spectra, corresponding to X-ray absorption near-edge structure analysis of the region, both without and with grinding, showing the resolved components of tri- and tetravalent cerium based on cerium fluoride(CeF_3) and tetravalent cerium oxide(CeO_2) as reference spectra, respectively.

3.3. Cerium Reduction by Mechanochemical Processing via Planetary Ball Milling

Details of the mechanochemical phenomenon, structural change analysis, and the mechanism of cerium reduction by mechanochemical processing via planetary ball milling have already been given in our previous papers [13,14]. Briefly, the valence of cerium without and with grinding samples is shown in Table 4. From Table 4, the concentration of trivalent cerium was significantly increased according to grinding time. After finishing

planetary ball milling, the temperature of the grinding sample was at a maximum of about 50 °C. Thus, it was confirmed that the cerium reduction reaction occurred during planetary ball milling as a mechanochemical reaction.

The results of structural change analysis corresponding to cerium reduction reaction are shown in Table 5 [14]. As shown in Table 5, the atomic distances of both Ce(IV)-O and Ce(III)-O decreased as the grinding time increased. This trend shows that the oxygen vacancy is generated in the structure of cerianite by planetary ball milling [33]. When an oxygen vacancy is generated in the structure of cerianite, it has been reported that the local structure around the oxygen vacancy becomes an A-type or B-type structure [14]. In addition, it was reported that when both A-type and B-type structures were generated in the structure of cerianite, the atomic distances of Ce(IV)-O and Ce(III)-O was decreased.

Table 4. Concentration of tri- and tetravalent cerium samples without and with grinding, based on the X-ray absorption near-edge structure analysis in cerium K-edge (%) [14].

Grinding Time (min)	Concentration of Trivalent Cerium	Concentration of Tetravalent Cerium
0	30.5	69.5
10	31.9	68.1
60	50.0	50.0
720	74.4	25.6

Table 5. Cerium fitting results of the radial distribution function for samples without and with grinding, assuming four kinds of cerium shells for tetravalent cerium oxide [14].

Sample	Shell	CN	R [× m^{-10}]	σ^2 [× m^{-20}]	ΔE_0
CeO_2	Ce(IV)-O	7.7	2.35	0.009	−10.3
	Ce(III)-O		-		
	Ce(III)-Ce(III)		-		
	Ce(IV)-Ce(IV)	12.2	3.84	0.005	
Without grinding	Ce(IV)-O	8.7	2.35	0.02	−9.3
	Ce(III)-O	0.2	2.46	0.04	
	Ce(III)-Ce(III)	0.3	3.81	0.002	
	Ce(IV)-Ce(IV)	12.1	3.83	0.008	
10 min grinding	Ce(IV)-O	8.0	2.36	0.02	−10.6
	Ce(III)-O	0.06	2.47	−0.01	
	Ce(III)-Ce(III)	0.2	3.81	0.001	
	Ce(IV)-Ce(IV)	11.4	3.84	0.008	
60 min grinding	Ce(IV)-O	4.0	2.31	0.006	2.4
	Ce(III)-O	3.9	2.42	0.02	
	Ce(III)-Ce(III)	7.4	3.77	0.008	
	Ce(IV)-Ce(IV)	5.4	3.79	0.009	
720 min grinding	Ce(IV)-O	0.1	2.30	0.009	−3.4
	Ce(III)-O	8.4	2.42	0.03	
	Ce(III)-Ce(III)	10.0	3.76	0.04	
	Ce(IV)-Ce(IV)	2.6	3.79	0.0009	

CN: coordination number; R (× m^{-10}): atomic distance; ΔE_0: threshold E_0 shift; σ^2 (× m^{-20}): Debye–Waller factor.

3.4. Cerium Reduction by Mechanochemical Processing via Grinding with Microwave Irradiation

The XAFS spectra at the cerium K-edge and the valence of cerium in samples without grinding, and then with grinding and microwave irradiation, are shown in Figure 3 and Table 6, respectively. When the valence of cerium is evaluated using XAFS analysis, the XAFS analysis at the cerium L_{III} edge has more advantages than at the cerium K-edge. However, we confirmed that the XAFS spectra at the cerium K-edge were sufficient to evaluate the valence of cerium in our previous paper [14]. Thus, we evaluated the valence of cerium using the XAFS spectra at the cerium K-edge.

The concentration of trivalent cerium significantly increased with grinding time, in the same way as planetary ball milling (Tables 4 and 6). Since the reaction temperature was fixed at 250 °C during grinding with microwave irradiation, it was confirmed that the cerium reduction reaction occurred as a mechanochemical reaction.

The k^3-weighted EXAFS spectra and RDF are shown in Figures 4 and 5, respectively. The curve fitting results are listed in Table 7 and are plotted in Figures 4 and 5. In RDF (Figure 5), the peak position of the four shells is shown. Since the contribution of a third shell (Ce(III)-Ce(III)) is quite minor, relative to that of a fourth shell (Ce(IV)-Ce(IV)) [14], the peak positions of both the third and fourth shells overlap. As shown in Table 7, the atomic distance of both Ce(IV)-O and Ce(III)-O decreased as the grinding time increased, in the same way as planetary ball milling. This trend is the same as that in planetary ball milling (Section 3.3). Thus, the structural change of cerianite by grinding with microwave irradiation showed that oxygen vacancies occurred in the structure. In addition, two tetravalent cerium structures surrounding the oxygen vacancy took an electron and were reduced to trivalent cerium when the oxygen vacancy occurred [14]. The cerium reduction mechanism caused by grinding with microwave irradiation was the same as that achieved by planetary ball milling [14].

Table 6. Concentration of tri- and tetravalent cerium in the samples by grinding with microwave irradiation, based on X-ray absorption near-edge structure analysis in the cerium K-edge (%).

Grinding Time (min)	Concentration of Trivalent Cerium	Concentration of Tetravalent Cerium
0	30.5	69.5
60	40.7	59.3
180	46.9	53.1
420	53.4	46.6

Table 7. Cerium fitting results assuming four kinds of cerium shell for tetravalent cerium oxide, samples by grinding with microwave irradiation in the radial distribution function.

Sample	Shell	CN	R [× m^{-10}]	σ^2 [× m^{-20}]	ΔE_0
CeO_2	Ce(IV)-O	7.7 ± 2.0	2.35	0.009	−10.3
	Ce(III)-O		-		
	Ce(III)-Ce(III)		-		
	Ce(IV)-Ce(IV)	12.2 ± 12.0	3.84	0.005	
Without grinding	Ce(IV)-O	8.7 ± 4.8	2.35	0.02	−9.3
	Ce(III)-O	0.2 ± 1.8	2.46	0.04	
	Ce(III)-Ce(III)	0.3 ± 3.8	3.81	0.002	
	Ce(IV)-Ce(IV)	12.1 ± 11.9	3.83	0.008	
60 min grinding	Ce(IV)-O	7.5 ± 1.8	2.35	0.003	2.6
	Ce(III)-O	0.6 ± 0.6	2.47	0.016	
	Ce(III)-Ce(III)	1.0 ± 1.2	3.81	0.005	
	Ce(IV)-Ce(IV)	11.4 ± 6.6	3.84	0.006	
180 min grinding	Ce(IV)-O	6.9 ± 4.8	2.29	0.025	−4.0
	Ce(III)-O	1.1 ± 0.7	2.41	−0.002	
	Ce(III)-Ce(III)	2.5 ± 1.0	3.75	0.008	
	Ce(IV)-Ce(IV)	10.2 ± 3.8	3.78	0.005	
420 min grinding	Ce(IV)-O	6.7 ± 13.1	2.21	0.063	−14.7
	Ce(III)-O	1.8 ± 12.0	2.32	0.00006	
	Ce(III)-Ce(III)	9.0 ± 4.9	3.66	0.004	
	Ce(IV)-Ce(IV)	3.4 ± 2.2	3.69	0.014	

Note that CN: coordination number; R (× m^{-10}): atomic distance; ΔE_0: threshold E_0 shift; σ^2 (× m^{-20}): Debye–Waller factor.

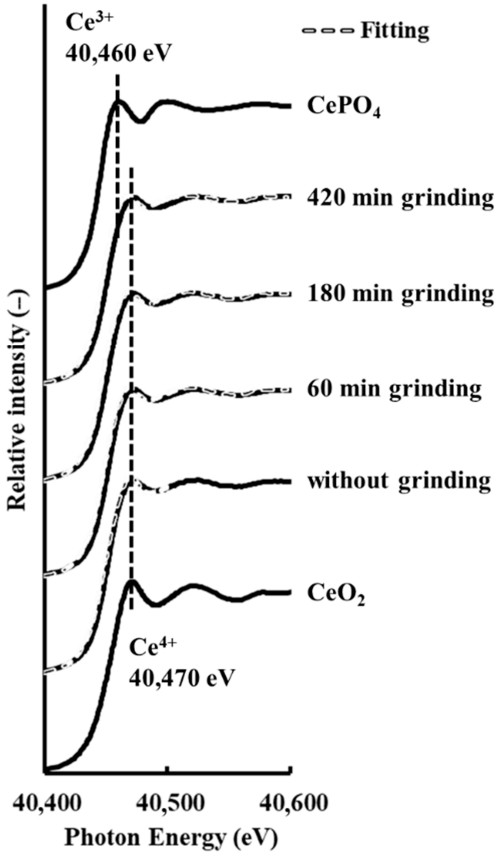

Figure 3. Cerium K-edge X-ray absorption fine structure spectra, corresponding to X-ray absorption near-edge structure analysis of the samples by grinding with microwave irradiation, showing resolved components of tri- and tetravalent cerium, based on cerium phosphate($CePO_4$) and tetravalent cerium oxide(CeO_2) as reference spectra, respectively.

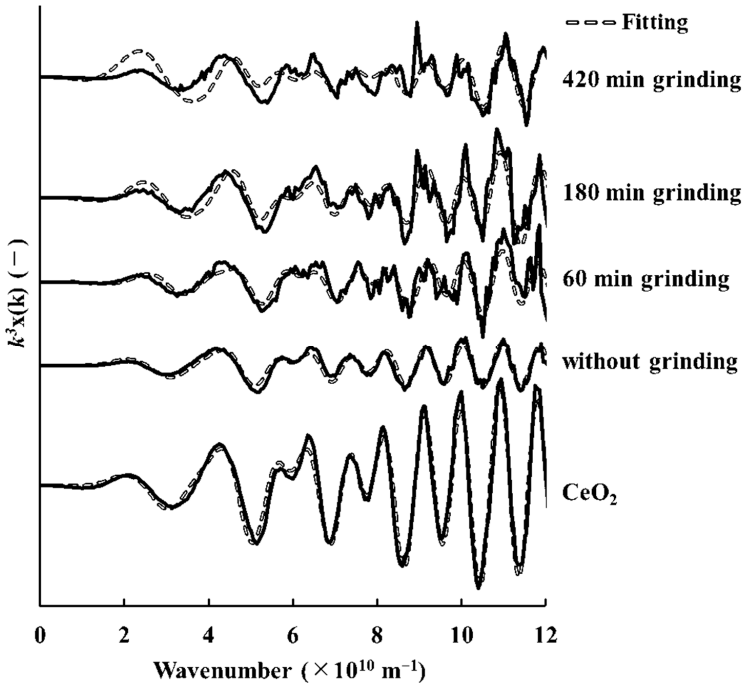

Figure 4. The k^3-weighted cerium K-edge extended X-ray absorption fine structure spectra of tetravalent cerium oxide, samples by grinding with microwave irradiation.

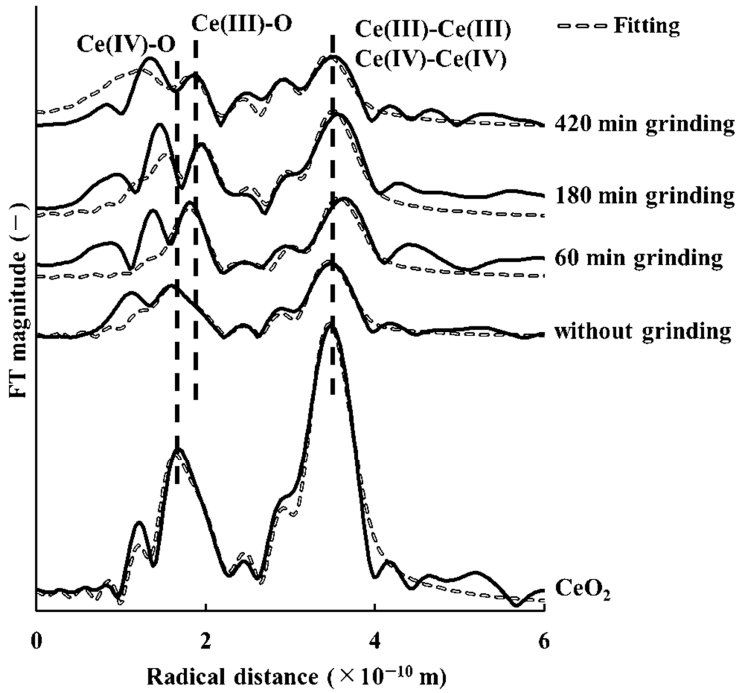

Figure 5. The radial distribution function of tetravalent cerium oxide, samples by grinding with microwave irradiation.

3.5. Comparison Cerium Reduction Efficiency among These Methods

The relationship between energy consumption and the amount of cerium reduction in each process is shown in Figure 6. When the energy consumption was the same in each process, the mechanochemical processing by grinding with microwave irradiation showed the highest amount of cerium reduction among these processes (Figure 6). This finding shows that mechanochemical processing by grinding with microwave irradiation using the agitator mixer could be conducted as a large-scale process more easily than that by planetary ball milling and microwave irradiation. As discussed in the Introduction, the development and optimization of attractive proof-of-principle laboratory experiments into viable large-scale processes have not been achieved since a planetary ball mill is commonly used not on a large scale but only on a laboratory scale. However, based on this result, it is possible that the development and optimization of attractive proof-of-principle laboratory experiments into large-scale processes could be conducted in mechanochemical processing by grinding with microwave irradiation using the agitator mixer. The method of heating and processing by microwave irradiation is the least effective since the amount of cerium reduction is the lowest. Ribeiro et al. [23] reported that microwave irradiation is not always advantageous, due to its rather complicated relationship with the composition of the reaction mixture, the reaction mechanism, and a number of other factors. Thus, it was confirmed that heat processing by microwave irradiation is not effective for this ore.

When the value of x is 1 in Equation (1), the equation of cerium reduction reaction changes to Equation (2). As described in Sections 3.3 and 3.4, the oxygen vacancy plays an important role in the cerium reduction reaction during planetary ball milling and grinding with microwave irradiation. Equation (2) can be substituted for the half-reaction equation (Equation (3)) involving oxygen vacancy (V_O) [34–36]:

$$2CeO_2 \rightarrow Ce_2O_3 + \frac{1}{2}O_2 \quad (2)$$

$$4Ce^{4+} + O^{2-} \rightarrow 2Ce^{4+} + 2Ce^{3+} + V_O + \frac{1}{2}O_2 \quad (3)$$

According to Equation (3), the amount of oxygen vacancy could be estimated by the amount of cerium reduction. As shown in Tables 4 and 6, we are able to evaluate the amount of cerium reduction from the XAFS analysis. The relationship between grinding time and the oxygen vacancy ratio in mechanochemical processing by both planetary ball milling and grinding with microwave irradiation is shown in Figure 7. In Figure 7, no significant difference between the mechanochemical processing by grinding with microwave irradiation and that by planetary ball milling was found in the oxygen vacancy ratio. This finding showed that the efficiency of cerium reduction by grinding with microwave irradiation was the same as that achieved by planetary ball milling. As shown in Table 7, the atomic distance of both Ce(IV)-O and Ce(III)-O by grinding with microwave irradiation decreased more than that by planetary ball milling. When the cerium reduction reaction occurs, oxygen vacancies are produced in the cerianite structure [14]. As a result of this structural change, the atomic distance of both Ce(IV)-O and Ce(III)-O decreases. Thus, the EXAFS results shown in Section 3.4 revealed that it was easier to change the structure of cerianite in weathered residual rare-earth ore by grinding it with microwave irradiation than by planetary ball milling. In addition, it was reported that the Ce(IV)-O distance of nanocrystalline CeO_2 was slightly shorter, with small CeO_2 particles, in the previous study [37]. Based on the above results, it is suggested that the structural change of cerianite by grinding with microwave irradiation contributed not only to the cerium reduction reaction but also to nanocrystallization.

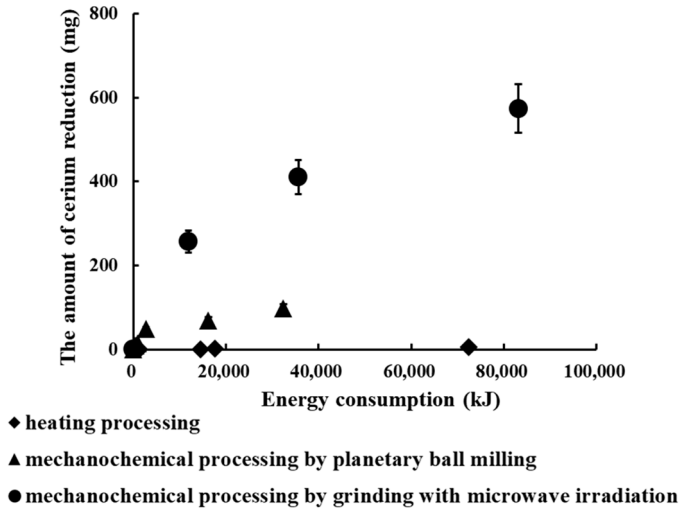

Figure 6. Relationship between energy consumption and the amount of cerium reduction.

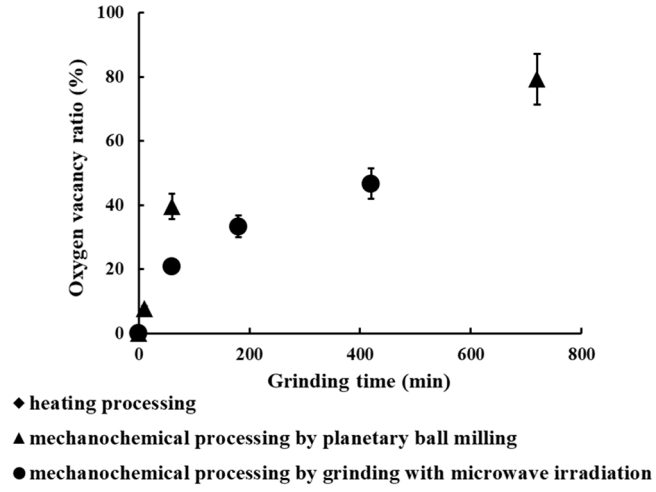

Figure 7. Relationship between grinding time and the oxygen vacancy ratio.

Based on the above results, the efficiency of cerium reduction by grinding with microwave irradiation was the same as that achieved by planetary ball milling. However, the amount of treatment involved in grinding with microwave irradiation is larger than that involved in planetary ball milling since the volume of the agitating mixer is 40 times that of the planetary ball mill. Thus, it was revealed that a large amount of tetravalent cerium could be reduced by grinding with microwave irradiation, with the same efficiency as that achieved by planetary ball milling.

4. Conclusions

As a result of EXAFS analysis, it was confirmed that the atomic distances of both Ce(III)–O and Ce(IV)–O in the structure of samples ground down by grinding with microwave irradiation decreased, which indicated that the oxygen vacancy reaction occurred. Since this trend is the same as that achieved by planetary ball milling, it was suggested that the cerium reduction mechanism by grinding with microwave irradiation was the same, based on the XAFS analysis results. Since the decrease in atomic distance achieved by grinding with microwave irradiation was bigger than that achieved by planetary ball milling, it was revealed that it was easier to change the structure of cerianite in weathered residual rare-earth ore by grinding with microwave irradiation than by planetary ball milling. In addition, it is suggested that the structural change of cerianite by grinding with microwave irradiation contributed not only to cerium reduction reaction but also to nanocrystallization. When evaluating the cerium reduction efficiency, it was revealed that a large amount of tetravalent cerium could be reduced by grinding with microwave irradiation, with the same efficiency as that achieved by planetary ball milling.

Author Contributions: Conceptualization, M.I.; C.T.; formal analysis, T.K.; investigation, T.K.; M.I.; resources, M.I.; writing—original draft preparation, T.K.; writing—review and editing, C.T.; supervision, C.T.; project administration, T.K.; C.T.; funding acquisition, C.T. All authors have read and agreed to the published version of the manuscript.

Funding: This research received no external funding.

Institutional Review Board Statement: Not applicable.

Informed Consent Statement: Not applicable.

Data Availability Statement: Data available on request due to restrictions eg privacy or ethical.

Acknowledgments: The synchrotron radiation experiments were performed using a BL5S1 beamline courtesy of the Aichi Synchrotron Radiation Center, Aichi Science & Technology Foundation, Aichi, Japan (Proposal No. 201801021), and a BL01B1 beamline of SPring-8, with the approval of the Japan Synchrotron Radiation Research Institute (Proposal No. 2021B1031). Part of this work was performed as a component of the activities of the Research Institute of the Sustainable Future Society, Waseda Research Institute for Science and Engineering, Waseda University.

Conflicts of Interest: The authors declare no conflict of interest.

References

1. Katsenis, A.D.; Puskaric, A.; Strukil, V.; Mottillo, C.; Julien, P.A.; Uzarevic, K.; Pham, M.H.; Do, T.O.; Kimber, S.A.J.; Lazic, P.; et al. In situ x-ray diffraction monitoring of a mechanochemical reaction reveals a unique topology metal-organic framework. *Nat. Commun.* **2015**, *6*, 6662. [CrossRef] [PubMed]
2. Balaz, P.; Takacs, L.; Luxova, M.; Godocikova, E.; Ficeriova, J. Mechanochemical processing of sulphidic minerals. *Int. J. Miner. Process.* **2004**, *74S*, S365–S371. [CrossRef]
3. Esmaeili, E.; Rounaghi, S.A.; Eckert, J. Mechanochemical synthesis of rosin-modified montmorillonite: A breakthrough approach to the next generation of OMMT/Rubber nanocomposites. *Nanocomposites* **2021**, *11*, 1974. [CrossRef] [PubMed]
4. Fan, E.; Li, L.; Zhang, X.; Bian, Y.; Xue, Q.; Wu, J.; Wu, F.; Chen, R. Selective recovery of Li and Fe from spent lithium-ion batteries by an environmentally friendly mechanochemical approach. *ACS Sustain. Chem. Eng.* **2018**, *6*, 11029–11035. [CrossRef]
5. Liu, K.; Liu, L.; Tan, Q.; Li, J. Selective extraction of lithium from a spent lithium iron phosphate battery by mechanochemical solid-phase oxidation. *Green Chem.* **2021**, *23*, 1344. [CrossRef]
6. Wang, G.W. Mechanochemical organic synthesis. *Chem. Soc. Rev.* **2013**, *42*, 7668. [CrossRef]

7. Li, Y.; Liu, Q.; Li, W.; Lu, Y.; Meng, H.; Li, C. Efficient destruction of hexachlorobenzene by calcium carbide through mechanochemical reaction in a planetary ball mill. *Chemosphere* **2017**, *166*, 275–280. [CrossRef]
8. Dallimore, M.P.; Mccormick, P.G. Dynamics of planetary ball milling: A comparison of computer simulated processing parameters with CuO/Ni displacement reaction milling kinetics. *Mater. Trans. JIM* **1996**, *37*, 1091–1098. [CrossRef]
9. Patil, P.R.; Kartha, K.P.R. Application of ball milling technology to carbohydrate reactions: I. regioselective primary hydroxyl protection of hexosides and nucleoside by planetary ball milling. *J. Carbohydr. Chem.* **2008**, *27*, 279–293. [CrossRef]
10. Yamamoto, K.; Garcia, S.E.B.; Muramatsu, A. Zeolite synthesis using mechanochemical reaction. *Microporous Mesoporous Mater.* **2007**, *101*, 90–96. [CrossRef]
11. Suzuki, M.; Iguchi, H.; Ohtani, A.; Hirota, M.; Oshima, T. Effect of grinding condition on hydrophobic surface-treatment of quarts sand using planetary mill. *Kagaku Kogaku Ronbunshu* **1995**, *21*, 111–117. [CrossRef]
12. Hiroshi, M. Estimation of mechanochemical reaction rate and optimum design of planetary ball mill by discrete element method. *J. Soc. Powder Technol. Jpn.* **2005**, *42*, 134–139.
13. Kato, T.; Granata, G.; Tsunazawa, Y.; Takagi, T.; Tokoro, C. Mechanism and kinetics of enhancement of cerium dissolution from weathered residual rare earth ore by planetary ball milling. *Miner. Eng.* **2019**, *134*, 365–371. [CrossRef]
14. Kato, T.; Tsunazawa, Y.; Liu, W.; Tokoro, C. Structural change analysis of cerianite in weathered residual rare earth ore by mechanochemical reduction using x-ray absorption fine structure. *Minerals* **2019**, *9*, 267. [CrossRef]
15. Kato, T.; Granata, G.; Tokoro, C. Evaluation of acids onto the light rare earth elements dissolution from weathered residual rare earth ore activated by mechanochemical treatment by grinding. *J. Soc. Powder Technol. Jpn.* **2019**, *56*, 174–180. [CrossRef]
16. Granata, G.; Takahashi, K.; Kato, T.; Tokoro, C. Mechanochemical activation of chalcopyrite: Relationship between activation mechanism and leaching enhancement. *Miner. Eng.* **2019**, *131*, 280–285. [CrossRef]
17. Minagawa, M.; Hisatomi, S.; Kato, T.; Granata, G.; Tokoro, C. Enhancement of copper dissolution by mechanochemical activation of copper ores: Correlation between leaching experiments and DEM simulations. *Adv. Powder Technol.* **2018**, *29*, 471–478. [CrossRef]
18. Mitani, Y.; Tsunazawa, Y.; Okura, T.; Tokoro, C. Enhancement of copper leaching from chalcopyrite using wet-type ball mill. *J. Soc. Powder Technol. Jpn.* **2015**, *52*, 723–729. [CrossRef]
19. Titscher, L.; Breitung, F.S.; Kwade, A. Experimental parametric study for dry grinding in planetary ball mills. *Chem. Ing. Tech.* **2016**, *88*, 1524–1529. [CrossRef]
20. Mio, H.; Kano, J.; Saito, F. Scale-up method of planetary ball mill. *Chem. Eng. Sci.* **2004**, *59*, 5909–5916. [CrossRef]
21. Stolle, A.; Schmidt, R.; Jacob, K. Scale-up of organic reactions in ball mills: Process intensification with regard to energy efficiency and economy of scale. *Faraday Discuss* **2014**, *170*, 267. [CrossRef] [PubMed]
22. Otani, N.; Furuya, T.; Katsuumi, N.; Haraguchi, T.; Akitsu, T. Synthesis of amino acid derivative Schiff base copper(II) complexes by microwave and wet mechanochemical methods. *J. Indian Chem. Soc.* **2021**, *98*, 100004. [CrossRef]
23. Ribeiro, A.P.C.; Alegria, E.C.B.A.; Kopylovich, M.N.; Ferraria, A.M.; Do, R.A.M.B.; Pombeiro, A.J.L. Comparison of microwave and mechanochemical energy inputs in the catalytic oxidation of cyclohexane. *Dalton Trans.* **2018**, *47*, 8193–8198. [CrossRef] [PubMed]
24. Rehr, J.J.; Albers, R.C.; Zabinsky, S.I. High-order multiple-scattering calculations of x-ray-absorption fine structure. *Phys. Rev. Lett.* **1992**, *69*, 3399–3400. [CrossRef]
25. Rehr, J.J. Recent developments in multiple-scattering calculations of XAFS and XANES. *Jpn. J. Appl. Phys.* **1993**, *32*, 8–12. [CrossRef]
26. Ravel, B.; Newville, M. Athena, artemis, hephaestus: Data analysis for x-ray absorption spectroscopy using IFEFFIT. *J. Synchrotron Radiat.* **2005**, *12*, 537–541. [CrossRef]
27. HSC Chemistry 5.0. *Chemical Reaction and Equilibrium Software with Extensive Hermochemical Database ver. 5.11*; Outokumpu Research Oy: Piori, Finland, 2002.
28. Bulfin, B.; Lowe, A.J.; Keogh, K.A.; Murphy, B.E.; Lubben, O.; Krasnikov, S.A.; Shvets, I.V. Analytical model of CeO_2 oxidation and reduction. *J. Phys. Chem. C* **2013**, *117*, 24129–24137. [CrossRef]
29. Trovarelli, A.; Fornasiero, P. *Catalysis by Ceria and Related Materials*, 2nd ed.; Imperial College Press: London, UK, 2013; pp. 1–881.
30. Skorodumova, N.V.; Simak, S.L.; Lundqvist, B.L.; Abrikosov, L.A.; Johansson, B. Quantum origin of the oxygen storage capability of ceria. *Phys. Rev. Lett.* **2002**, *89*, 166601. [CrossRef]
31. Silva, J.L.F.D. Stability of the Ce_2O_3 phases: ADFT +Uinvestigation. *Phys. Rev. B* **2007**, *76*, 193108. [CrossRef]
32. Bartos, A.; Lieb, K.P.; Uhrmacher, M.; Wiarda, D. Refinement of atomic positions in bixbyite oxide using perturbed angular correlation spectroscopy. *Acta Crystallogr. Sect. B* **1993**, *49*, 165–169. [CrossRef]
33. Badlducci, G.; Kaspar, J.; Fornasiero, P.; Graziani, M.; Islam, M.S.; Gale, J.D. Computer simulations studies of bulk reduction and oxygen migration in CeO_2-ZrO_2 solid solutions. *J. Phys. Chem.* **1997**, *101*, 1750–1753. [CrossRef]
34. Haneda, M.; Mizushima, T.; Kakuta, N.; Ueno, A.; Sato, Y.; Matsuura, S.; Kasahara, K.; Sato, M. Structural characterization and catalytic behavior of Al_2O_3-supported cerium oxides. *Bull. Chem. Soc. Jpn.* **1993**, *66*, 1279–1288. [CrossRef]
35. Ghigna, P.; Spinolo, G.; Scavini, M.; Tamburini, U.A.; Chadwick, A.V. The atomic and electronic structure of cerium substitutional defects in $Nd_{2-x}Ce_xCuO_{4+\delta}$ an XAS study. *Phys. C Supercond.* **1995**, *253*, 147–155. [CrossRef]

36. Koettgen, J.; Martin, M. Coordination numbers in Sm-doped ceria using x-ray absorption spectroscopy. *J. Phys. Chem. C* **2019**, *123*, 6333–6339. [CrossRef]
37. Lee, J.F.; Tang, M.T.; Shih, W.C.; Liu, R.S. Ce K-edge EXAFS study of nanocrystalline CeO_2. *Mater. Res. Bull.* **2002**, *37*, 555–562. [CrossRef]